

Deterministic, scalable, and entanglement efficient initialization of arbitrary quantum states

Prithvi Gundlapalli and Junyi Lee*

*Institute of Materials Research and Engineering,
Agency for Science, Technology and Research (A*STAR),
2 Fusionopolis Way, #08-03 Innovis, 138634 Singapore*

(Dated: October 27, 2021)

Quantum computing promises to provide exponential speed-ups to certain classes of problems. In many such quantum algorithms, a classical vector \mathbf{b} is encoded in the amplitudes of a quantum state $|b\rangle$. However, efficient amplitude encoding of an arbitrary vector \mathbf{b} in $|b\rangle$ is known to be a difficult problem that can reverse the gains of such algorithms. More importantly, an arbitrary quantum state of Q qubits generally requires $\sim 2^Q$ number of entangling gates, which is problematic for today’s Noisy-Intermediate Scale Quantum (NISQ) computers where large numbers of such error-prone gates will result in significant decoherence before initialization is completed. In this work, we demonstrate a deterministic and scalable initialization algorithm that allows for states with low entanglement to be initialized on actual quantum computers with more than an order of magnitude fewer entangling gates and significantly shallower circuits as compared to isometric decomposition. For states with higher entanglement, optimally approximate states with lower entanglement may be found and initialized with similar performance. We show this to be true for various cases of interest such as the normal and log-normal distributions. Unlike variational approaches, our method requires no classical optimizations in high dimensional spaces and is not plagued with exponentially vanishing gradients or a multitude of local minimas.

I. INTRODUCTION

The inefficient initialization of quantum states is a bottleneck that currently prevents many quantum algorithms from achieving quantum supremacy over their classical counterparts. For example, the exponential speed-up of the Harrow-Hassidim-Lloyd (HHL) [1] algorithm presumes the existence of an efficient way to encode the components of a classical vector \mathbf{b} in the amplitudes of a quantum state $|b\rangle$. However, such an oracle remains elusive. Beyond HHL, amplitude encoding is used in many other diverse areas including singular value estimation [2], least-squares fitting [3], and machine learning such as support vector machines [4] and autoencoders [5]. All these algorithms presume accurate state preparation but initialization circuits that are overly deep threaten to introduce unacceptable decoherence in today’s NISQ computers [6], resulting in an unusable set of states that hinders correct execution of the main algorithm. It is therefore vitally important to have an efficient, robust, and scalable initialization sub-routine.

Over the years, numerous initialization schemes have been proposed, including initialization via factorization of the Hilbert space [7], decomposition of isometries [8], quantum generative adversarial networks (qGAN) [9, 10], variational quantum circuits [11, 12], and matrix product states (MPS) inspired approaches [13, 14]. However, these methods all suffer from various problems and are less than ideal. Variational methods, like qGAN and most variational quantum circuits, use a fixed circuit ansatz with parametrized gates that are progressively

tuned through iterative optimization steps to achieve the target state. Although these approaches have enjoyed some success in initializing relatively small quantum registers (~ 3 qubits), their general applicability is still doubtful for several reasons. Firstly, optimization of these circuits require the use of a loss function, but it is known that the gradient of many loss functions vanish exponentially for large system sizes, making it extremely difficult for the optimizer to make any progress [15]. Secondly, besides vanishing gradients, numerical experiments also suggest that the loss function’s landscape is pockmarked with a multitude of local minima, making the optimizer’s task even more challenging [16]; in the supplementary material, we present results from some of our own numerical experiments that also support this finding [17]. Thirdly, there is no compelling reason to choose one circuit topology over another and since there is no guarantee that the chosen ansatz will eventually yield the desired state, it is difficult to know when to stop optimizing and to try a different topology instead. While attempts have been made to also optimize the circuit’s topology [12, 18], it is likely that this will only aggravate the severeness of the optimization problem when scaled to larger system size. Finally, we note that in all these variational approaches, there is an unspecified cost of classical training time, which could well negate the theorized speed-up of quantum algorithms.

In contrast to these variational methods, there are other analytical approaches that do not require intense optimizations and whose results are mathematically guaranteed (in an ideal noiseless quantum computer). They are, in that sense, “deterministic” as compared to variational methods where there is no guarantee of a solution’s existence given a specified circuit topol-

* lee_jun_yi@imre.a-star.edu.sg

ogy. The chief disadvantage of these methods is that exact initialization of an arbitrary Q -qubit state generally requires $\sim 2^Q$ entangling gates [7, 8, 19], which is prohibitively expensive in the NISQ era. More recently, there have been proposals to shorten the depth of these circuits by utilizing additional ancillary qubits [20]. Nevertheless, it should be noted that the final state of such routines is entangled with the ancillary qubits. Consequently, it cannot be accepted by all algorithms expecting a usual amplitude encoding without additional modifications or measurements.

A common deficiency of all the initialization routines discussed thus far is their insensitivity to the entanglement of the target state. By this we mean that although a generic Q -qubit state may require an exponential number of entangling gates to initialize, it is clear that not every state requires such extensive resources to prepare. Indeed, a product state with no entanglement can be prepared with a single layer of non-entangling single qubit gates, but current deterministic approaches do not explicitly account for this difference between states and can, as we show in section IV, potentially use an order of magnitude more entangling gates than necessary. Furthermore, although a highly entangled state may require a substantial number of entangling gates, it is worth asking if one might find an optimally approximate state (in the amplitudes of the state) that has lower entanglement, and is therefore easier to initialize with less entangling gates. This is a pertinent question in the NISQ era because one might ironically achieve higher fidelity to the target state by initializing to an approximate state than by attempting an exact initialization with significantly larger numbers of entangling gates.

In this paper, we utilize the properties of matrix product states to adaptively initialize arbitrary states with varying degrees of entanglement. Although previous attempts to use matrix product states for initialization were limited to specific types of states, and/or were unable to exactly initialize states with arbitrary degrees of entanglement [13, 14], our method is free from any such limitations. Furthermore, our approach only utilizes nearest-neighbor entangling gates, which is important when implementing on actual hardware with constraints on qubit connectivity [21], and it only uses such gates sparingly when the entanglement of the target state calls for it. Moreover, it is scalable because we only require one such gate per qubit. Our method is most efficient when applied to states with low entanglement. For states with higher entanglement, similar performance may be obtained when initializing to an optimally approximate state with lower entanglement. We demonstrate superior performance over initialization via isometric decomposition on actual NISQ computers for both these cases. The rest of the paper is structured as follows: in section II, we review relevant properties of matrix product states, and in section III, we describe the details of our initialization algorithm. In section IV, we benchmark our approach on IBM's quantum computers against a standard determin-

istic initialization routine on Qiskit [22] that uses isometric decomposition. Finally, we conclude in section V.

II. MATRIX PRODUCT STATES

Matrix product states, or tensor-trains as they are known in the computational mathematics literature [23, 24], are used widely for many applications including generative modeling in machine learning [25], estimation of singular values [26], studying of phase transitions in field theories [27], and perhaps most famously, in the density matrix renormalization group technique for studying 1-dimensional quantum many-body systems [28]. At the heart of a MPS is the re-writing of the expansion coefficients $A(j_1, \dots, j_Q)$ of the Q -body state $\sum_{j_1, \dots, j_Q} A(j_1, \dots, j_Q) |j_Q, \dots, j_1\rangle$ into a sum-product of Q , 3-dimensional tensors $A_{\alpha^{n-1}, j_n, \alpha^n}^n$ (also sometimes referred to as a MPS *core*)

$$|\psi\rangle = \sum_{\substack{j_1 \dots j_Q \\ \alpha^0 \dots \alpha^Q}} A_{\alpha^0, j_1, \alpha^1}^1 A_{\alpha^1, j_2, \alpha^2}^2 \dots A_{\alpha^{Q-1}, j_Q, \alpha^Q}^Q \times |j_Q, \dots, j_1\rangle, \quad (1)$$

where the α^n are summation indices (also known as *virtual* or *bond* indices) with dimensions $\dim(\alpha^n) \in \mathbb{N}$ for $1 \leq n < Q$, $n \in \mathbb{N}$, and $\dim(\alpha^0) = \dim(\alpha^Q) = 1$. As written above, j_n can be any quantum number and are frequently referred to as *physical* indices in MPS parlance. However, we shall now exclusively let j_n refer to the computational basis state of the n^{th} qubit, and $\dim(j_n)$ is therefore always 2. More generally, we shall use lowercase latin alphabets to represent physical indices and greek letters to label bond indices. Numerical superscripts are used to enumerate the $Q + 1$ different bond indices while numerical subscripts shall identify a particular qubit. We shall also refer to the α^{n-1} and α^n bond indices of $A_{\alpha^{n-1}, j_n, \alpha^n}^n$ as the *left* and *right* bond indices of A^n respectively.

Although Eq. (1) may seem to be a trivial re-writing of the expansion coefficients, MPSs have several nice features that give additional physical intuition to the initialization problem. For example, the dimension of the bond indices α^n is proportional to the entanglement between the bi-partition $\{j_1, \dots, j_n\}$ and $\{j_{n+1}, \dots, j_Q\}$ [29]. In particular, if $\dim(\alpha^n) = 1$ for all n , then we see from Eq. (1) that the state is a separable product state with no entanglement. Moreover, if the range of $\dim(\alpha^n)$, $1 \leq n < Q$, is not restricted, then it can be shown that the state of a Q -qubit system can always be written as a MPS [24, 29], or in other words, a MPS can describe states of arbitrarily high entanglement. Analytical decomposition of the expansion coefficients $A(j_1, \dots, j_Q)$ into a sum-product of MPS cores are known for only a few special cases [30], but decomposition of A can always be accomplished numerically via successive singular-value decompositions (SVD) [24, 29].

Since we wish to emphasize that our approach works for arbitrary quantum states, we briefly illustrate how this is accomplished. Moreover, it highlights a simple way in which locally optimal approximations to the target state can be systematically achieved.

We begin by noting that the expansion coefficients $A(j_1, \dots, j_Q)$ can always be reshaped into a matrix. We shall use the notation $A(j_1, \dots, j_Q)$ to denote A as a Q -dimensional tensor, and $A(j_1, \dots, j_n; j_{n+1}, \dots, j_Q)$ as a matrix with $\prod_{i=1}^n \dim(j_i)$ rows and $\prod_{i=n+1}^Q \dim(j_i)$ columns. Given the expansion coefficients $A(j_1, \dots, j_Q)$, we then perform the following series of SVD and reshaping operations

$$\begin{aligned}
A(j_1, \dots, j_Q) &= \sum_{\alpha^1} U(j_1; \alpha^1) B(\alpha^1; j_2, j_3, \dots, j_Q) \\
&= \sum_{\alpha^1} A_{\alpha^0, j_1, \alpha^1}^1 B(\alpha^1; j_2; j_3, \dots, j_Q) \\
&= \sum_{\alpha^1 \alpha^2} A_{\alpha^0, j_1, \alpha^1}^1 U(\alpha^1, j_2; \alpha^2) B(\alpha^2; j_3, \dots, j_Q) \\
&= \sum_{\alpha^1 \alpha^2} A_{\alpha^0, j_1, \alpha^1}^1 A_{\alpha^1, j_2, \alpha^2}^2 B(\alpha^2; j_3; j_4, \dots, j_Q) \\
&\quad \vdots \\
&= \sum_{\alpha^0 \dots \alpha^Q} A_{\alpha^0, j_1, \alpha^1}^1 A_{\alpha^1, j_2, \alpha^2}^2 \dots A_{\alpha^{Q-1}, j_Q, \alpha^Q}^Q. \quad (2)
\end{aligned}$$

In the first line, we have reshaped $A(j_1, \dots, j_Q)$ into a matrix $B(j_1; j_2, \dots, j_Q)$ and performed a SVD so that $B(j_1; j_2, \dots, j_Q) = \sum_{\alpha^1} U(j_1; \alpha^1) B(\alpha^1; j_2, j_3, \dots, j_Q)$. Notice that $\dim(\alpha^1)$ is the number of columns of U , and is also the number of singular values. Next, we reshape $U(j_1; \alpha^1)$ into the first of our desired MPS core $A_{\alpha^0, j_1, \alpha^1}^1$ (recall that $\dim(\alpha^0) = 1$), and the matrix $B(\alpha^1; j_2, j_3, \dots, j_Q)$ with $\dim(\alpha^1)$ rows into a matrix $B(\alpha^1, j_2; j_3, \dots, j_Q)$ with $\dim(\alpha^1) \times \dim(j_2)$ rows. We then perform a SVD on $B(\alpha^1, j_2; j_3, \dots, j_Q)$ in the third line, and an analogous reshaping operation on the fourth line. This process is then iterated until $A(j_1, \dots, j_Q)$ is fully decomposed into Q MPS cores as desired. Equivalently, we may view this as a series of Schmidt decompositions, with the number of Schmidt coefficients (dimension of α^n) at the n^{th} decomposition giving a measure of the entanglement between the bi-partitions $\{j_1, \dots, j_n\}$ and $\{j_{n+1}, \dots, j_Q\}$ [29, 31].

This explicit decomposition suggests a natural and easy way to make locally optimal approximations: at each n^{th} SVD step, keep only the k_n largest singular values

$$\begin{aligned}
B(\alpha^{n-1}, j_n; j_{n+1}, \dots, j_Q) &\equiv B_n \\
&= \sum_{\alpha^n=1}^{r_n} U(\alpha^{n-1} j_n; \alpha^n) B(\alpha^n; j_{n+1}, \dots, j_Q) \\
&\approx \sum_{\alpha^n=1}^{k_n} U(\alpha^{n-1} j_n; \alpha^n) B(\alpha^n; j_{n+1}, \dots, j_Q) \equiv B_{k_n}. \quad (3)
\end{aligned}$$

From the Eckart-Young theorem [32], this is locally optimal in the sense that B_{k_n} is the best k_n rank approximation to B_n (as defined in Eq. (3)) under both the Frobenius and spectral norm, with the error in the Frobenius norm simply given by the quadrature sum of the truncated singular values. Although the Eckart-Young theorem provides for an easy way to obtain a locally optimal approximation, we emphasize that this might not be globally optimal since the $n+1^{\text{th}}$ truncation is dependent on the n^{th} truncation, and the Eckart-Young theorem does not in that case guarantee that the final tensor is the best approximation to $A(j_1, \dots, j_Q)$. This can be a significant problem if the errors introduced at each truncation step is large. In that case, a variational approach to the truncation can be employed to find the globally optimal approximation to $A(j_1, \dots, j_Q)$ [33]. In this work, we were able to obtain satisfactory results with a simple truncation, but we note that variational truncation of the original MPS will generally lead to improved approximations. Physically, we should understand these truncations as effectively finding optimally approximate states (in the Frobenius norm of the expansion coefficients $A(j_1, \dots, j_Q)$) that have lower entanglement than the original state. Intuitively, we expect that such states should require less entangling gates and be easier to initialize. As we shall show in the rest of the paper, this is indeed so.

Besides giving a nice physical intuition of the entanglement present between various sub-partitions, another nice feature of the MPS form in Eq. (1) is its locality. By locality we mean here that Eq. (1) separates out the expansion coefficients' dependence on the physical indices (qubits) such that an MPS core can be said to belong to a particular qubit that only "interacts" with its neighboring core through the contraction of its left and right bond indices. As we shall also see later, this will allow us to initialize a state with only nearest-neighbor gates. This is important when implementing the algorithm on actual NISQ-era hardware with limited qubit connectivity because it minimizes the number of noisy SWAP operations required.

Lastly, we note that the decomposition of $A(j_1, \dots, j_Q)$ into the MPS form is not unique. One easy way to see this is to recognize that at each SVD in Eq. (2), we may insert the identity $I = X X^{-1}$ (where X is any unitary matrix) in between U and B and re-define $U X \rightarrow U$, $X^{-1} B \rightarrow B$ such that each $A_{\alpha^{n-1}, j_n, \alpha^n}^n$ in the decomposition can be changed without altering the quantum state. This gauge freedom allows a MPS state to be transformed such that the cores A^n for $1 < n \leq Q$ obey the orthonormal relations

$$\sum_{j_n, \alpha^n} A_{\alpha^{n-1}, j_n, \alpha^n}^n A_{\beta^{n-1}, j_n, \alpha^n}^{n*} = \delta_{\alpha^{n-1}, \beta^{n-1}}. \quad (4)$$

Moreover, if the MPS state is normalized, A^1 also obeys the relation

$$\sum_{j_1, \alpha^1} A_{\alpha^0, j_1, \alpha^1}^1 A_{\alpha^0, j_1, \alpha^1}^{1*} = 1. \quad (5)$$

A MPS state that obeys these relations is said to be a *right-canonical* MPS [33]. For the rest of the paper, we shall assume that our MPS state is in the right-canonical form. Any MPS obtained through an exact MPS decomposition can be transformed into a right-canonical form. However, the requirement that the MPS state is right-normalizable places limits on the truncated approximate MPS states. In particular, the dimension of the left bond index of A^n must obey the inequality

$$\dim(\alpha^{n-1}) \leq \dim(j_n) \dim(\alpha^n) = 2 \dim(\alpha^n). \quad (6)$$

To see why this is true, we note that the right normalization relations (Eq. (4) and (5)) can be interpreted to mean that each A^n core has $\dim(\alpha^{n-1})$ orthogonal $\mathbb{C}^{\dim(j_n) \times \dim(\alpha^n)}$ vectors. Since a $\mathbb{C}^{\dim(j_n) \times \dim(\alpha^n)}$ vector space cannot have more than $\dim(j_n) \times \dim(\alpha^n)$ orthogonal vectors, the inequality Eq. (6) naturally follows.

III. MATRIX PRODUCT INITIALIZER

We now turn to the actual work of initializing an arbitrary quantum state that has been expressed as a right-canonical MPS. Previously, Ran showed how a MPS consisting of cores with bond dimensions of 2 may be initialized with a fixed sequence of 2-qubit and 1-qubit gates [13]. However, this sequence was unable to exactly initialize MPSs with cores of arbitrary bond dimensions, which limits the usefulness of the technique. Here, we show how MPSs with cores of arbitrary bond dimensions may be initialized, which implies that any arbitrary state may be initialized using our technique. More importantly, it also allows for optimally approximate states with lower entanglement than the original state to be initialized, which can be very useful in the current NISQ era.

The problem of initialization may be described as finding a unitary matrix U such that $U|0, \dots, 0\rangle = |\psi\rangle$, where $|\psi\rangle$ is the desired target state to initialize. There is however no unique solution to U . This is plain if we view initialization of a Q qubit state as a rotation of one point $(|0, \dots, 0\rangle)$ to another $(|\psi\rangle)$ on a 2^Q dimensional sphere; clearly, there are infinitely many ways this may be accomplished. On a gate-based quantum computer, U must be formed from the product of several d -qubit gates, where $d \in \mathbb{N}$, $d \leq Q$. However, multi-qubit gates are experimentally difficult to implement and error-prone in the NISQ era. We therefore seek to find a U that only uses $d > 1$ qubit gates when “absolutely necessary”. By “absolutely necessary”, we mean that in general, $d > 1$ qubit gates are only needed when there is significant entanglement in the target quantum state. After all, a separable product state can be initialized with just one layer of 1 qubit gates. We thus want a U that is made out of variable d qubit gates with $d > 1$ only when the entanglement of the state calls for it. Moreover, it is plain that every qubit needs at least one gate to operate on it. Consequently, we write down as an ansatz that U can be given by the

quantum circuit that is shown in Fig. 1. Essentially, the ansatz consists of Q sequential d_n -qubit gates operating on the n^{th} to $n + d_n - 1^{\text{th}}$ qubit for $n = 1, \dots, Q$. We denote the unitary matrix represented by these gates as $G^{[n, d_n]}$. Notice that the ansatz is linear in the number of qubits. Moreover, although it is sequential as shown in Fig. 1, it can potentially be parallelized for appropriate values of d_n . For example, if $d_n = 1$ for all n , then the ansatz is simply one layer of 1-qubit gates. Lastly, we point out that although the circuit in Fig. 1 seems to suggest some restriction on d_n (for example, $G^{[Q-1, d_{Q-1}]}$ cannot have $d_n > 2$), this is as we shall show later, not a limitation.

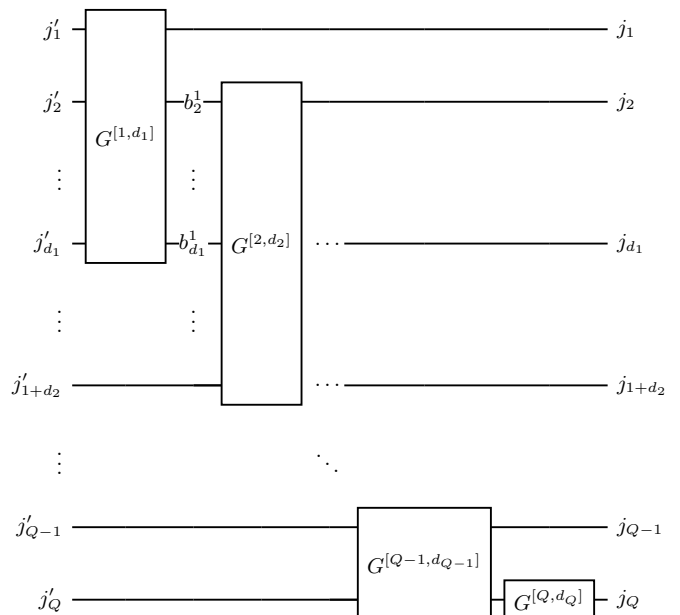


Figure 1. Matrix product initializer ansatz for Q qubits consisting of Q sequential (potentially multi-qubit) gates. Each gate $G^{[n, d_n]}$ is a d_n -qubit gate operating on the n^{th} to $n + d_n - 1^{\text{th}}$ qubit, where d_n depends on the state’s entanglement. j'_n are input states, j_n are the final output states, and b_n^m are intermediate states.

Armed with this ansatz, we may write down the unitary matrix of each gate in the initializer. For the first gate, we have

$$G^{[1, d_1]} = \sum_{\substack{j'_1 \dots j'_{d_1} \\ j_1 b_2^1 \dots b_{d_1}^1}} G^{[1, d_1]}(b_{d_1}^1, \dots, b_2^1, j_1; j'_{d_1}, \dots, j'_1) \times |b_{d_1}^1, \dots, b_2^1, j_1\rangle \langle j'_{d_1}, \dots, j'_1|. \quad (7)$$

Consistent with our notation above, j'_n above denotes the initial quantum number of the n^{th} qubit (typically 0). On the other hand, j_n is the final quantum number of the n^{th} qubit after initialization. This is distinct from b_n^m , which is an intermediate quantum number of the n^{th} qubit after operation of the m^{th} gate (see Fig. 1).

Likewise, for $n = 2, \dots, Q - 1$, $G^{[n, d_n]}$ has the form

$$G^{[n, d_n]} = \sum_{ij} G^{[n, d_n]}(i; j) |i\rangle \langle j|, \quad (8)$$

where

$$i = b_{n+d_{n-1}}^n, \dots, b_{n+1}^n, j_n, \quad (9)$$

and

$$j = \begin{cases} b_{n+d_{n-1}}^{n-1}, \dots, b_n^{n-1}, & \text{for } d_{n-1} - 1 = d_n \\ j'_{n+d_{n-1}}, \dots, j'_{n+d_{n-1}-1}, b_{n+d_{n-1}-2}^{n-1}, \dots, b_n^{n-1}, & \\ & \text{for } d_{n-1} - 1 < d_n. \end{cases} \quad (10)$$

Notice that we have not in Eq. (10) defined j for the case where $d_{n-1} - 1 > d_n$. As we will show later, this particular case is unnecessary, but for now we have for $G^{[Q, d_Q]}$

$$G^{[Q, d_Q]} = \sum_j G^{[Q, d_Q]}(j_Q; j) |j_Q\rangle \langle j|, \quad (11)$$

where

$$j = \begin{cases} b_Q^{Q-1}, & \text{for } d_{Q-1} = 2 \\ j'_Q, & \text{for } d_{Q-1} = 1. \end{cases} \quad (12)$$

The unitary matrix U is then

$$U = \sum_{\substack{j_1 \dots j_Q \\ j'_1 \dots j'_Q \\ \{b^1\} \dots \{b^{Q-1}\}}} G^{[Q, d_Q]} G^{[Q-1, d_{Q-1}]} \dots G^{[1, d_1]} \\ \times |j_Q \dots j_1\rangle \langle j'_Q \dots j'_1|. \quad (13)$$

In the summation above, we have used the notation $\{b^m\}$ to mean the set of all b indices with superscript equal to m . In other words, all the intermediate quantum numbers are summed over in Eq. (13). Also, since $G^{[n, d_n]}$, as defined in Eq. (7), (8), and (11) are 2^{d_n} -dimensional matrices, but U in Eq. (13) is 2^Q -dimensional, we have implicitly assumed in Eq. (13) that each $G^{[n, d_n]}$ has been appropriately expanded via the correct Kronecker products in accordance to the qubits that it operates on.

For initialization, we want $U |0, \dots, 0\rangle = |\psi\rangle$, where $|\psi\rangle$ is a right-canonical MPS as in Eq. (1). More precisely, we want U such that

$$\sum_{\{b^1\} \dots \{b^{Q-1}\}} G^{[Q, d_Q]} G^{[Q-1, d_{Q-1}]} \dots G^{[1, d_1]} \\ = A(j_1, \dots, j_Q), \quad (14)$$

when $j'_n = 0$ for all n . Here, we are viewing A as a tensor and the $G^{[n, d_n]}$ are in their “native” space. Comparing Eq. (14) with Eq. (2), we observe that in both cases, we have Q free indices (j_1, \dots, j_Q), Q MPS cores and gates, as well as $Q - 1$ non-trivial summation indices, which suggests that Eq. (14) can be accomplished

through a mapping between each n^{th} MPS core and gate. For this mapping to occur, we need to ensure that the space spanned by $\{b^n\}$ is at least as large as $\dim(\alpha^n)$. This can be enforced by choosing

$$d_n = 1 + \lceil \log_2 \dim(\alpha^n) \rceil. \quad (15)$$

This choice of d_n also ensures that $d_{n-1} - 1 \leq d_n \forall n$ so that our omission of the case $d_{n-1} - 1 > d_n$ in Eq. (10) is justified. To see this, we note that for any right-canonical MPS, the inequality Eq. (6) must hold. Taking \log_2 and adding one to both sides of the inequality, we have after rounding up

$$1 + \log_2 \lceil \dim(\alpha^{n-1}) \rceil \leq 2 + \lceil \log_2 \dim(\alpha^n) \rceil \\ \implies d_{n-1} - 1 \leq d_n. \quad (16)$$

Physically, the choice of d_n in Eq. (15) means that the number of qubits the n^{th} gate operates on is directly dependent on the entanglement between the subsystems $\{j_1, \dots, j_n\}$ and $\{j_{n+1}, \dots, j_Q\}$. For example, if $\dim(\alpha^n) = 1 \forall n$, i.e. the target state is a product state, then $d_n = 1 \forall n$ by Eq. (15), and the circuit reduces to simply one layer of 1-qubit gates. Thus our circuit by construction only uses $d > 1$ gates when the entanglement of the target state calls for it. Moreover, since $\dim(\alpha^Q) = 1$, this construction implies that the Q^{th} gate must be a 1-qubit gate. Similarly, the $Q - 1^{\text{th}}$ gate can at most be a 2-qubit gate, and so on. However, this limitation is not an issue because as we shall soon see, the circuit is capable of initializing any right-canonical MPS, and by extension, any quantum state.

It remains to prescribe the mapping from a MPS core A^n to a gate $G^{[n, d_n]}$. We begin by observing that each MPS core can be reshaped into a matrix $A^n(\alpha^{n-1}; \alpha^n, j_n) = A^n(i; j)$. In converting a multi-index like α^n, j_n into a single index j , we shall adopt a C-indexing convention, that is, indices on the right (j_n in this case) are incremented first before those on the left (α^n in this case). Each A^n core can thus be viewed as a matrix with $\dim(\alpha^{n-1})$ rows and $2 \dim(\alpha^n)$ columns. Now by construction, $G^{[n, d_n]}$ has at least $\dim(\{b^{n-1}\}) \geq \dim(\alpha^{n-1})$ columns [34]. Furthermore, it has $2 \dim(\{b^n\}) \geq 2 \dim(\alpha^n)$ rows [35]. We can therefore map the $\dim(\alpha^{n-1})$ rows of $A^n(\alpha^{n-1}; \alpha^n, j_n)$ into the first $\dim(\alpha^{n-1})$ columns of $G^{[n, d_n]}$, zero-padding any remaining rows. With this accomplished, any remaining columns of $G^{[n, d_n]}$ can be filled by requiring that $G^{[n, d_n]}$ is unitary, as is necessary for a quantum gate. To do this, we note that since the MPS is right-canonical, each of the $\dim(\alpha^{n-1})$, $2 \dim(\alpha^n)$ -dimensional row vector in A^n are orthonormal to each other. Consequently, a trivial embedding of them in a potentially larger $2 \dim(\{b^n\})$ -dimensional space by zero-padding the extra dimensions will mean that they are still orthonormal in the larger space. We thus have $\dim(\alpha^{n-1})$ filled columns that are orthonormal vectors in a $\mathbb{C}^{2 \dim(\{b^n\})}$ vector space, and $2 \dim(\{b^n\}) - \dim(\alpha^{n-1})$ remaining columns to fill

such that $G^{[n,d_n]}$ is unitary. Clearly, this can be accomplished by filling the still empty columns with the remaining $2 \dim(\{b^n\}) - \dim(\alpha^{n-1})$ orthonormal vectors in $\mathbb{C}^{2 \dim(\{b^n\})}$.

We have now by explicit construction shown that our circuit ansatz, comprising of a sequence of Q (potentially multi-qubit) gates, is capable of initializing any arbitrary state of a Q qubit system. In the next section, we benchmark our algorithm on real quantum computers via IBM’s open access quantum cloud services.

IV. HARDWARE BENCHMARKING

Although our algorithm is capable of initializing arbitrary states, its real utility in the NISQ era is its ability to very efficiently initialize states with low entanglement. This degree of entanglement for a Q qubit system can be quantified with the mean normalized bipartite entropy, which we define as

$$\bar{S} = \left\langle \frac{S(\rho_n)}{\min(n, Q - n)} \right\rangle = \left\langle -\frac{\text{Tr}(\rho_n \log_2 \rho_n)}{\min(n, Q - n)} \right\rangle, \quad (17)$$

where $\rho_n \equiv \text{Tr}_n(\rho)$ is the reduced density matrix of the sub-partition $\{j_1, \dots, j_n\}$, and the average is over all sub-partitions $\{j_1\}$, $\{j_1, j_2\}$, \dots , $\{j_1, \dots, j_{Q-1}\}$. Note that $S(\rho_n)/\min(n, Q - n)$ is just the normalized bipartite von Neumann entropy, which is a measure of the entanglement between the bipartitions $\{j_1, \dots, j_n\}$ and $\{j_{n+1}, \dots, j_Q\}$, with zero indicating a separable state and one indicating a maximally entangled state. \bar{S} , which ranges between zero and one, is therefore the average normalized bipartite von Neumann entropy over all bipartitions of the system. Generally speaking, our algorithm yields the most savings in terms of gate count and circuit depth compared to other deterministic methods when \bar{S} is small.

An example of a target state with a relatively low mean normalized bipartite entropy is the sinusoidal probability distribution shown in Fig. 2d, with $\bar{S} = 0.076$. In this case, we were able to exactly initialize the target distribution with an order of magnitude less CNOT gates and with a circuit that is shallower by about three times (details in Table I) compared to Qiskit’s isometric initialization that is based on [8]. Not surprisingly, our algorithm was also able to achieve a higher fidelity, which can be visualized in Fig. 2d that shows the target distribution in a solid blue line, as well as the measured probability distribution obtained via our algorithm (green crosses) and isometric decomposition (red pluses). Error bars shown in this and other plots give the expected 1-sigma deviation of the measured probabilities based on the number of shots and theoretical probability of obtaining each state. In all our tests, we simply chose the least busy quantum hardware at execution time without special consideration for the error rate and qubit connectivity and we have used the standard transpilation routine on Qiskit with the highest level of optimization.

Initializing sparse vectors is of particular interest to quantum algorithms like HHL and it is therefore interesting to see if our method can generate substantial savings in such cases. To test this, we randomly generated a vector with a sparsity of 0.9 where both the location and magnitude of the non-zero elements were randomly chosen. Although not every sparse vector will necessarily have low \bar{S} , some sparse vectors may have very low entropy, and in this case, our algorithm can enable significantly better results over isometric initialization. For example, the sparse vector state visualized in Fig. 2c has a very low \bar{S} of 0.014, and in this case, we were able to exactly initialize the state with just 2 CNOT gates, compared to 70 with an isometric decomposition. This is a striking demonstration of the utility of entanglement-sensitive routines like ours. With a circuit depth that is more than six times shallower than isometric decomposition, we were able to achieve a significantly higher fidelity of 0.959 over 0.717.

For states with larger entanglement, optimally approximate states can be found using the procedure outlined in section II, and using this approximate state, our method can sometimes still achieve better fidelities than initialization via existing deterministic methods. In the first row of Fig. 2, we compare our initialization of a normal (a) and log-normal (b) distribution, which are both of interest to the quantum finance community [36–39]. In both cases, the target probability distributions are plotted as blue solid lines while their matrix product state approximations are given by orange dots. As discussed in section II, these are states that are optimally (in the Frobenius norm) approximate to the target state but with lower entanglement [40]. The truncation of singular values for the normal distribution can be visualized as in Fig. 3. To ensure a fair comparison, the isometric initialization shown in Fig. 2a and Fig. 2b were also used to initialize the same approximate MPS target state as our algorithm. However, as Table I shows, there is actually little difference in the experimental fidelity of the isometric method when it initializes to the exact target state instead. This is not surprising since the isometric decomposition does not specifically optimize based on the entanglement of the target state. We emphasize that although our algorithm initialized to an approximate state, it nevertheless performs substantially better than an exact initialization using isometric decomposition as the results in Table I shows. In particular, for the case of the normal distribution in Fig. 2a, our method used more than an order of magnitude less CNOT gates, with about 2.5 times shallower depth, and achieved a significantly higher fidelity to the target state.

V. CONCLUSION

Arbitrary quantum states are difficult to prepare with high fidelities on today’s NISQ computers. Due to noise from multi-qubit entangling gates, deep quantum circuits

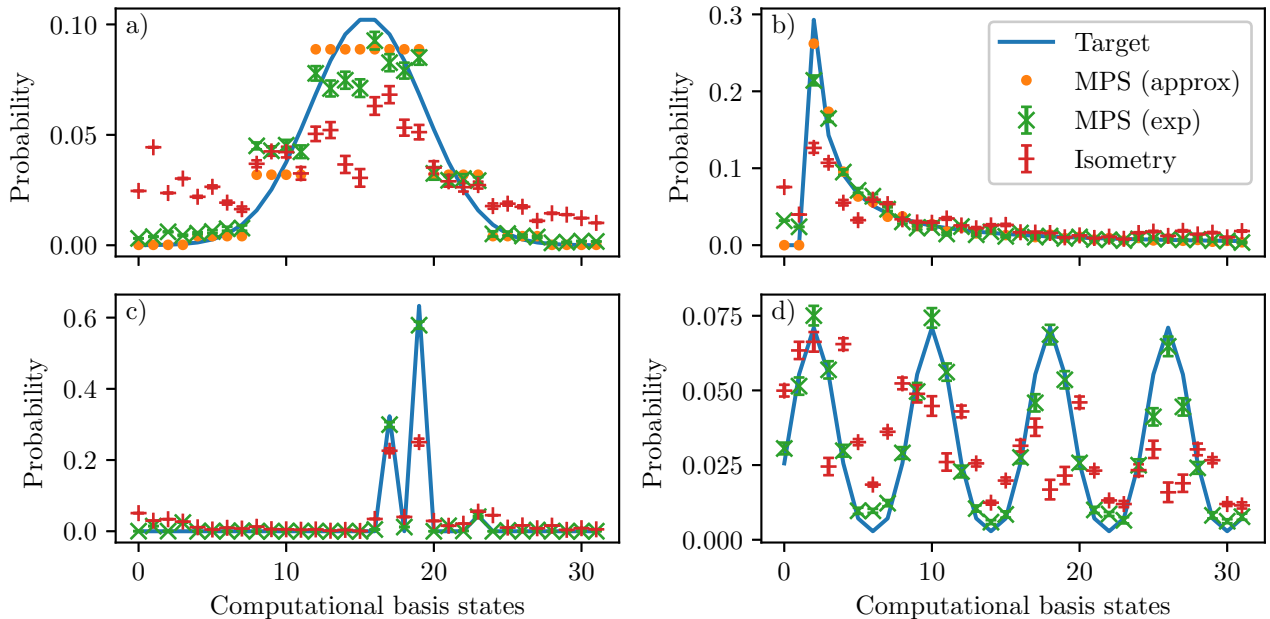


Figure 2. (color online) Initialization of various probability distributions on IBM’s quantum computers: (a) normal distribution, (b) log-normal distribution, (c) a “random” distribution (see text for more details), and (d) a sinusoidal distribution. Blue solid lines demarcate the target probability distribution, while orange dots (if present) show the locally optimal approximate state with lower entanglement. Green crosses show experimental results obtained with our routine while red pluses show those obtained using isometric decomposition. Error bars give the theoretical 1-sigma spread of the measured probabilities.

Distribution	Hardware	Method	CNOT	R_z	SX	Circuit depth	Fidelity (exp)	Fidelity (theory)	Mean normalized bipartite entropy
Normal	ibmq_santiago	Ours (approx)	5	35	30	44	0.980	0.990	0.283
		Isometry (approx)	71	62	55	122	0.872	0.990	0.283
		Isometry (exact)	77	65	49	123	0.864	1	0.322
Log-normal	ibmq_santiago	Ours (approx)	9	45	44	57	0.967	0.998	0.192
		Isometry (approx)	73	78	68	144	0.907	0.998	0.192
		Isometry (exact)	63	66	51	129	0.917	1	0.206
Random	ibmq_santiago	Ours (exact)	2	17	17	22	0.959	1	0.014
		Isometry (exact)	70	72	61	140	0.717	1	0.014
Sinusoidal	ibmq_manila	Ours (exact)	5	30	28	40	0.995	1	0.076
		Isometry (exact)	57	65	61	118	0.921	1	0.076

Table I. Benchmark of our initialization algorithm compared to isometric decomposition. Gate (CNOT, R_z , and SX) counts and circuit depth for each method, as well as their experimentally measured fidelity to the target state are tabulated. When initialization to an approximate state is used, the fidelity of the approximate state to the exact state is listed under “Fidelity (theory)” (an entry with 1 means the exact state was used). The mean normalized bipartite entropy of the exact target state, defined in Eq. (17), is also given.

with a large number of such gates rapidly become incoherent and useless. Although analytical methods to exactly prepare arbitrary states have been known for a while, these approaches suffer from deep circuits and high entangling gate counts that increase exponentially with the number of qubits. This translates in practice to significant decoherence of the qubits that make them unusable for further computation. In response to this, variational circuits with parametrized gates have since been proposed for state preparation. Nevertheless, these cir-

cuits are not a panacea and are instead plagued with their own problems. For example, finding the loss function’s global minimum in these methods is highly challenging due to the curse of dimensionality, gradients that vanish exponentially with the number of qubits, and a proliferation of local minimas in the loss function’s landscape. More importantly, there is no obvious guiding principle for the selection of the circuit’s topology, and there is no guarantee that any given parametrized circuit will actually be able to prepare the state exactly. Furthermore,

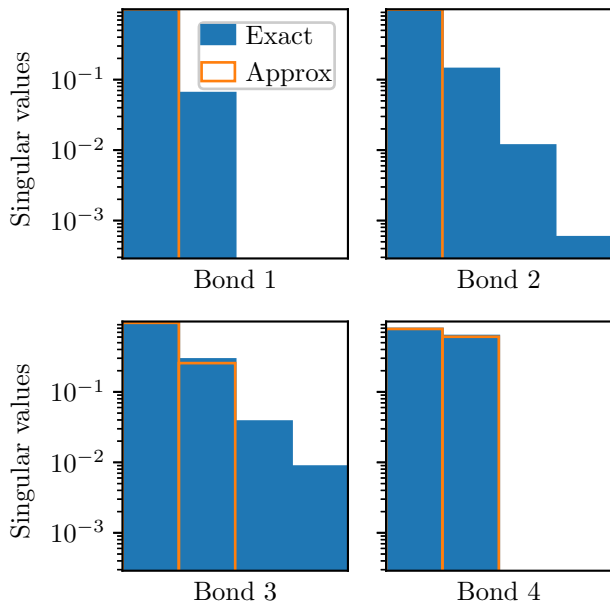


Figure 3. (color online) Singular values from the decomposition of the normal distribution in Fig. 2a. Filled blue bars show all singular values in the exact decomposition. The approximate state (orange dots in Fig. 2a) was obtained by keeping only the singular values outlined with orange lines.

none of these existing approaches take into account the fact that states with less entanglement should in theory be easier to prepare with less entangling gates.

In this work, we have developed an initialization circuit that uses only the same number of nearest-neighbor gates as the number of qubits, which minimizes the number of expensive SWAP operations due to limited qubit connectivity. Although each of these nearest-neighbor gates may be an expensive multi-qubit gate that further decomposes into multiple one and two-qubit gates, our routine only uses such gates sparingly when the entanglement of the target state calls for them. In cases where a target state (or a sub-system of it) is separable, our

circuit automatically takes advantage of this by utilizing single qubit gates and parallelizing gate operations where possible. In short, our initialization routine allows states with less entanglement to be prepared far more efficiently compared to other deterministic but entanglement insensitive methods such as isometric decomposition. For states with low entanglement, our tests on actual quantum computers hosted on IBM’s cloud service show that our circuit is capable of achieving higher initialization fidelities compared to standard isometric decomposition by utilizing an order of magnitude less CNOT gates and having a significantly shallower circuit. For states with higher entanglement, we can still sometimes achieve significantly better performance by initializing to an optimally approximate state with lower entanglement, including states that represent a normal and log-normal distribution. Finally, we emphasize that unlike variational approaches, our method does not require challenging minimizations in a high dimensional space where the existence of a solution is uncertain, and exponentially vanishing gradients and a multitude of local minima make progress towards a global minimum difficult. Our initialization circuit is therefore an extremely valuable tool in the NISQ era for preparing arbitrary states with acceptable fidelities without having to incur significant classical optimization costs.

ACKNOWLEDGMENTS

The authors acknowledge Aravind Anthur and Leonid Krivitsky’s contributions in securing grant QEP-SF2 from the Quantum Engineering Programme in Singapore that provided financial support for this work. Numerical experiments in the supplementary material were conducted with the resources of A*STAR Computational Resource Center (A*CRC), with the Python libraries Dask [41], CuPy [42], and Numba [43] used for parallelization and acceleration. Quantum circuit simulations and executions were performed using Qiskit [22].

-
- [1] A. W. Harrow, A. Hassidim, and S. Lloyd, Quantum algorithm for linear systems of equations, *Phys. Rev. Lett.* **103**, 150502 (2009).
 - [2] L. Wossnig, Z. Zhao, and A. Prakash, Quantum linear system algorithm for dense matrices, *Phys. Rev. Lett.* **120**, 050502 (2018).
 - [3] N. Wiebe, D. Braun, and S. Lloyd, Quantum algorithm for data fitting, *Phys. Rev. Lett.* **109**, 050505 (2012).
 - [4] P. Rebentrost, M. Mohseni, and S. Lloyd, Quantum support vector machine for big data classification, *Phys. Rev. Lett.* **113**, 130503 (2014).
 - [5] J. Romero, J. P. Olson, and A. Aspuru-Guzik, Quantum autoencoders for efficient compression of quantum data, *Quantum Science and Technology* **2**, 045001 (2017).
 - [6] J. Preskill, Quantum computing in the NISQ era and beyond, *Quantum* **2**, 79 (2018).
 - [7] M. Plesch and C. Brukner, Quantum-state preparation with universal gate decompositions, *Phys. Rev. A* **83**, 032302 (2011).
 - [8] R. Iten, R. Colbeck, I. Kukuljan, J. Home, and M. Christandl, Quantum circuits for isometries, *Phys. Rev. A* **93**, 032318 (2016).
 - [9] C. Zoufal, A. Lucchi, and S. Woerner, Quantum generative adversarial networks for learning and loading random distributions, *npj Quantum Information* **5**, 103 (2019).
 - [10] H. Situ, Z. He, Y. Wang, L. Li, and S. Zheng, Quantum generative adversarial network for generating discrete distribution, *Information Sciences* **538**, 193–208 (2020).

- [11] W. W. Ho and T. H. Hsieh, Efficient variational simulation of non-trivial quantum states, *SciPost Phys.* **6**, 29 (2019).
- [12] L. Cincio, K. Rudinger, M. Sarovar, and P. J. Coles, Machine learning of noise-resilient quantum circuits, *PRX Quantum* **2**, 010324 (2021).
- [13] S.-J. Ran, Encoding of matrix product states into quantum circuits of one- and two-qubit gates, *Phys. Rev. A* **101**, 032310 (2020).
- [14] A. Holmes and A. Y. Matsuura, Efficient quantum circuits for accurate state preparation of smooth, differentiable functions (2020), [arXiv:2005.04351 \[quant-ph\]](https://arxiv.org/abs/2005.04351).
- [15] M. Cerezo, A. Sone, T. Volkoff, L. Cincio, and P. J. Coles, Cost function dependent barren plateaus in shallow parametrized quantum circuits, *Nature Communications* **12**, 10.1038/s41467-021-21728-w (2021).
- [16] A. G. R. Day, M. Bukov, P. Weinberg, P. Mehta, and D. Sels, Glassy phase of optimal quantum control, *Phys. Rev. Lett.* **122**, 020601 (2019).
- [17] See Supplementary Material at URL for numerical studies of local minima affecting variational circuits.
- [18] L. Cincio, Y. Subaşı, A. T. Sornborger, and P. J. Coles, Learning the quantum algorithm for state overlap, *New Journal of Physics* **20**, 113022 (2018).
- [19] V. Bergholm, J. J. Vartiainen, M. Möttönen, and M. M. Salomaa, Quantum circuits with uniformly controlled one-qubit gates, *Phys. Rev. A* **71**, 052330 (2005).
- [20] I. F. Araujo, D. K. Park, F. Petruccione, and A. J. da Silva, A divide-and-conquer algorithm for quantum state preparation, *Scientific Reports* **11**, 6329 (2021).
- [21] F. Leymann and J. Barzen, The bitter truth about gate-based quantum algorithms in the NISQ era, *Quantum Science and Technology* **5**, 044007 (2020).
- [22] M. S. Anis *et al.*, *Qiskit: An open-source framework for quantum computing* (2021).
- [23] S. Holtz, T. Rohwedder, and R. Schneider, The alternating linear scheme for tensor optimization in the tensor train format, *SIAM Journal on Scientific Computing* **34**, A683 (2012).
- [24] I. V. Oseledets, Tensor-train decomposition, *SIAM Journal on Scientific Computing* **33**, 2295 (2011).
- [25] Z.-Y. Han, J. Wang, H. Fan, L. Wang, and P. Zhang, Unsupervised generative modeling using matrix product states, *Phys. Rev. X* **8**, 031012 (2018).
- [26] N. Lee and A. Cichocki, Estimating a few extreme singular values and vectors for large-scale matrices in tensor train format, *SIAM Journal on Matrix Analysis and Applications* **36**, 994 (2015).
- [27] A. Milsted, J. Haegeman, and T. J. Osborne, Matrix product states and variational methods applied to critical quantum field theory, *Phys. Rev. D* **88**, 085030 (2013).
- [28] U. Schollwöck, The density-matrix renormalization group, *Rev. Mod. Phys.* **77**, 259 (2005).
- [29] G. Vidal, Efficient classical simulation of slightly entangled quantum computations, *Phys. Rev. Lett.* **91**, 147902 (2003).
- [30] I. V. Oseledets, Constructive representation of functions in low-rank tensor formats, *Constructive Approximation* **37**, 1 (2013).
- [31] A. Ekert and P. L. Knight, Entangled quantum systems and the schmidt decomposition, *American Journal of Physics* **63**, 415 (1995).
- [32] C. Eckart and G. Young, The approximation of one matrix by another of lower rank, *Psychometrika* **1**, 211 (1936).
- [33] S. Paeckel, T. Köhler, A. Swoboda, S. R. Manmana, U. Schollwöck, and C. Hubig, Time-evolution methods for matrix-product states, *Annals of Physics* **411**, 167998 (2019).
- [34] For $G^{[1,d_1]}$, it has at least 2 columns from j'_1 and $\dim(\alpha^0) = 1$, so it also has more columns than $\dim(\alpha^{n-1})$.
- [35] For $G^{[Q,d_Q]}$, it has 2 rows from j_Q and $\dim(\alpha^Q) = 1$, so its number of rows is equal to $2 \dim(\alpha^n)$.
- [36] P. Rebentrost, B. Gupt, and T. R. Bromley, Quantum computational finance: Monte carlo pricing of financial derivatives, *Phys. Rev. A* **98**, 022321 (2018).
- [37] S. Woerner and D. J. Egger, Quantum risk analysis, *npj Quantum Information* **5**, 15 (2019).
- [38] D. J. Egger, R. Garcia Gutierrez, J. Cahue Mestre, and S. Woerner, Credit risk analysis using quantum computers, *IEEE Transactions on Computers*, 1 (2020).
- [39] N. Stamatopoulos, D. J. Egger, Y. Sun, C. Zoufal, R. Iten, N. Shen, and S. Woerner, Option Pricing using Quantum Computers, *Quantum* **4**, 291 (2020).
- [40] The optimality is only local in this case since no variational truncation was employed.
- [41] Dask Development Team, *Dask: Library for dynamic task scheduling* (2016).
- [42] R. Okuta, Y. Unno, D. Nishino, S. Hido, and C. Loomis, Cupy: A numpy-compatible library for nvidia gpu calculations, in *Proceedings of Workshop on Machine Learning Systems (LearningSys)* (2017).
- [43] S. K. Lam, A. Pitrou, and S. Seibert, Numba: A llvm-based python jit compiler, in *Proceedings of the Second Workshop on the LLVM Compiler Infrastructure (LLVM '15)* (Association for Computing Machinery, New York, NY, USA, 2015).

Supplementary material for “Deterministic, scalable, and entanglement efficient initialization of arbitrary quantum states”

Prithvi Gundlapalli and Junyi Lee*
*Institute of Materials Research and Engineering,
 Agency for Science, Technology and Research (A*STAR),
 2 Fusionopolis Way, #08-03 Innovis, 138634 Singapore*
 (Dated: October 27, 2021)

I. INTRODUCTION

As discussed in the main text, variational initialization circuits suffer from vanishing gradients for large numbers of qubits and a lack of clear guidelines to motivate the selection of a circuit topology. In addition to these problems, our numerical experiments here also suggest that many initialization loss functions are plagued with a multitude of local minima that make it difficult to find the global minimum.

To numerically study these local minima, we attempt to initialize a few target states with the variational circuits shown in Fig 1. Local minima of a loss function are found by randomly initializing parameters in a variational circuit and optimizing them via a loss function and local optimizer (Limited-memory Broyden–Fletcher–Goldfarb–Shanno was used because our benchmarks showed that it was the fastest for our problem). For the most part, we used a binary-cross-entropy (BCE) loss function although other loss functions were also studied.

BCE is commonly used in machine learning tasks involving a binary classification of data. For N qubits, with 2^N states in the computational basis, the target probabilities of each basis state i is denoted y_{t_i} and the actual ‘measured’ (simulated in our case) probability of the basis states in our variational circuit is denoted y_{v_i} . A definition of BCE is given in Eq. 1

$$BCE = \sum_{i=1}^{2^N} y_{t_i} \log y_{v_i} + (1 - y_{t_i}) \log (1 - y_{v_i}). \quad (1)$$

Our 5 qubit variational ansatz circuit is shown in Fig. 1. We chose it as it contains a low number of CNOT gates that scales linearly with the number of qubits. We randomly initialize the 10 R_y gate parameters, θ_0 to θ_9 , and then use machine learning to determine the values of these parameters that would produce the desired initialization.

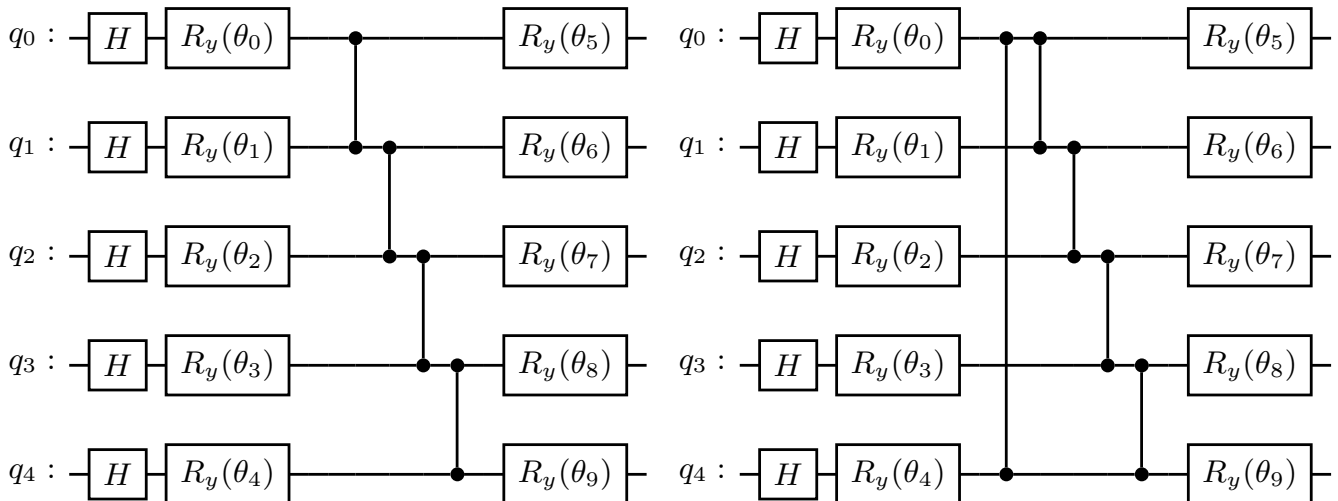


Figure 1. Our 5 qubit variational ansatz with a linear entanglement strategy (left) and circular entanglement strategy (right).

* lee_jun_yi@imre.a-star.edu.sg

We analyze our results by clustering the local minima in two ways: by their city block distance in parameter space, and the fidelity of the final state. Clustering in parameter space gives us a sense of the distribution of local minima within the parameter space of the variational circuit. On the other hand, clustering the local minima by the fidelity of their final state gives a measure of the uniqueness of each local minima in generating a particular final state. In general, one would hope for the existence of many well separated parameters that yield the target state since that would imply an easier optimization task for the optimizer.

For an N qubit variational circuit of the form in Fig. 1, the city block distance for two sets of optimized parameters θ_a and θ_b is as given in Eq. 2

$$\sum_{i=1}^{2N} |\theta_{a_i} - \theta_{b_i}|. \quad (2)$$

One must also be careful when computing the city block distance in this way since the parameters follow modular arithmetic rules outside of $-\pi$ to π and the circular distance must instead be considered. For instance, the points at $-\frac{4}{5}\pi$ and $\frac{4}{5}\pi$ are only $\frac{2}{5}\pi$ apart and not $\frac{8}{5}\pi$ apart since the angles wrap around. This also means that the maximum distance that two points can be separated by is π . Furthermore, the optimizer used in the learning algorithm was not constrained by any bounds to allow it to explore parameter values smaller than $-\pi$ or larger than π as these were still valid values. This must also be accounted for when computing the city block distance. Clustering in this manner is a computationally expensive task as a distance matrix has to be computed and an iterative algorithm must be used to ensure that all points within a distance δ of each other are considered a cluster.

II. RESULTS

In this section, we discuss some of the techniques we used when investigating this method and also the challenges faced.

In order to find the best solution (i.e. global minimum), one can only do an exhaustive search. Practically, one would have to sufficiently discretize the parameter space and optimize the circuit from as many possible combination of parameters as possible. This does not scale well. Our 5 qubit ansatz circuit has 10 free parameters that could vary from $-\pi$ to π . If we discretize each parameter to take just 5 values, that results in $5^{10} \approx 10$ million different sets of parameters. To make the problem somewhat more tractable, we settled on using 400,000 sets of random parameters (henceforth referred to as 400,000 *points*).

For all the results shown here, an ideal noiseless quantum circuit simulator was used to simulate a circuit's outcome.

A. Spread Of Local Minima

We discuss the results for a 5-qubit, 2-period sine initialization with a variational circuit employing a linear entanglement strategy. A distance clustering tolerance δ of 0.1 and a fidelity clustering tolerance of 0.999 was used to determine the criteria for clustering points together. The summary of results is shown in Table I.

	Distance	Fidelity
Number of Clusters	137,807	17,014
Largest Cluster Size	89	71,342
Total Size of Largest 10 Clusters	874	232,813
Number of Clusters with 1 Point	95,508	14,238
Mean Cluster Size \pm s.d.	2.9 ± 7.0	23.5 ± 734.0

Table I. Summary of distance and fidelity clustering for a 5 qubit circuit, 2-period sine wave initialization, linear entanglement strategy, 400,000 random points.

The same table for the normal distribution initialization target is shown in Table II.

The trend of the results for the 2-period sine wave target is the same as that of the normal distribution target and so we choose to elaborate on the 2-period sine wave initialization statistics only. We see that there are almost as many distance clusters as there are points, indicating that we very rarely converge to the same point when starting from a different point. In other words, we frequently converge to a different local minima when starting from a different initial

	Distance	Fidelity
Number of Clusters	190,461	17,226
Largest Cluster Size	60	92,050
Total Size of Largest 10 Clusters	538	274,196
Number of Clusters with 1 Point	135,252	14,101
Mean Cluster Size \pm s.d.	2.1 ± 3.9	23.2 ± 989.7

Table II. Summary of distance and fidelity clustering for a 5 qubit circuit, normal distribution initialization, linear entanglement strategy, 400,000 random points.

point. Also, the number of clusters with only 1 point in them is fairly large, indicating that our parameter space was not sufficiently discretized i.e. 400,000 points is not enough to consider this an ‘exhaustive’ search of the space. Ideally, a smallest cluster size of 2 points would likely indicate that the parameter space had been exhaustively searched as every point had converged to an already-known local minimum. This also implied that even better solutions could possibly exist using this circuit, but finding them would not be computationally feasible.

The 17,014 fidelity clusters indicate that there are at least that many ‘unique’ local minima (‘unique’ as in they result in the same state initialization) encountered by the learning algorithm. Interestingly, the large number of points (over 58%) contained in the biggest 10 fidelity clusters indicates that we converged to the same 10 state initializations more than half the time. We can see how large the first few fidelity clusters are in Fig. 2. Of the remaining points, about

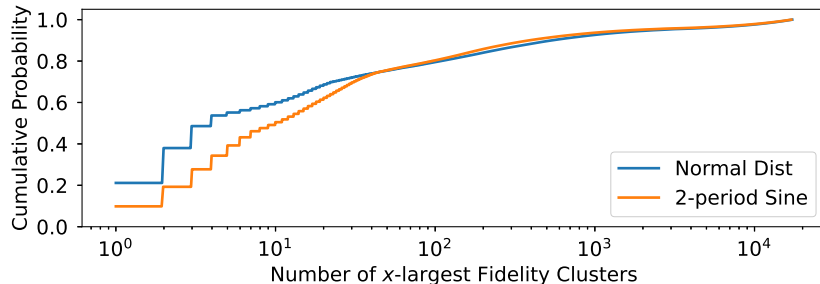


Figure 2. (color online) Cumulative probability of fidelity cluster sizes for the normal distribution (blue solid line) and 2-period sine targets (orange solid line). The x -axis is simply the number of x -largest fidelity clusters.

8.5% were in clusters that only had 1 point, which still represents a sizable number of ‘unique’ state initializations that were only encountered once. Again, this suggests that the parameter space has not been exhaustively searched. The significantly fewer fidelity clusters than distance clusters also suggests that points that produced the same outcome were not near each other in parameter space, and manual examination of the points within each fidelity cluster revealed that they were scattered all over parameter space. In other words, there exist multiple well separated local minima that produced a similar output state.

To better understand the distribution of good solutions (i.e. lower loss solutions), we can look at the cumulative probability of the distance cluster losses in Fig. 3. We see that the better solutions occur more often for the 2-period sine target than for the normal distribution target.

A histogram of the clustering results for a 2-period sine initialization is shown in Fig. 4 and the same for a normal distribution initialization is shown in Fig 5. The loss values were calculated using BCE, even for the fidelity clustering technique where the BCE loss was computed using the average statevector of all final states produced by circuits in that fidelity cluster. This was done to provide a common scale for comparison.

Although it appears that the fidelity clustering for the 2-period sine in Fig. 4 has ‘lost’ the lower loss solutions that the distance clustering produced, this is an artifact due to an insufficient fidelity clustering tolerance of 0.999. We note here that there are differences in the computation of distance clustering and fidelity clustering centroids. Whereas the distance clustering centroids can be computed from the mean of the parameters within the cluster, the representative statevector of a fidelity cluster centroid is not computed from the mean of all parameters within the cluster, but rather by the mean output statevector of the cluster. This is because parameters within a fidelity cluster could be scattered across the parameter space and their mean would not necessarily produce an output statevector that is representative of the fidelity cluster. Consequently, if a sufficiently high clustering tolerance is not used, the fidelity cluster centroid (i.e. mean statevector of all the points in the cluster) could exhibit a *worse* BCE loss than that of the individual points in the cluster.

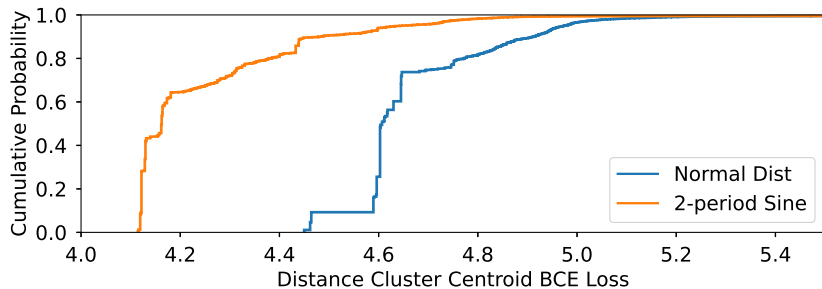


Figure 3. (color online) Cumulative probability of distance cluster BCE losses for the normal distribution (blue solid line) and 2-period sine (orange solid line) targets.

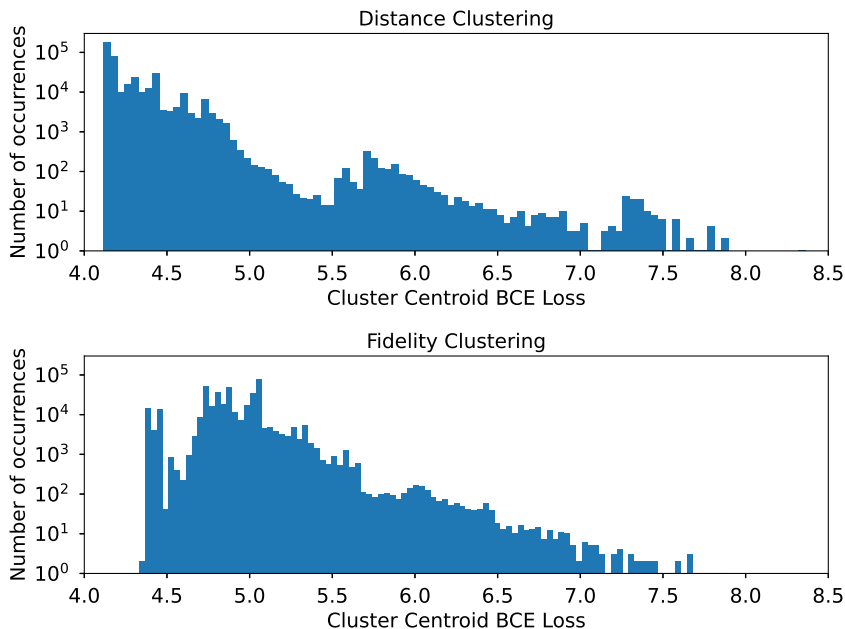


Figure 4. (color online) 2-period sine initialization target. (Top) The distance clustering histogram. (Bottom) The fidelity clustering histogram.

B. Escape Strategies

Our results show that even with 400,000 randomly initialized points, the parameter space has not yet been exhaustively searched and that lower-loss solutions could potentially be found. Moreover, the fact that there are large numbers of distance clusters imply that the loss function landscape is generally pockmarked with a multitude of local minima, which makes finding the global minimum difficult. Despite trying various strategies to alleviate this, none of our attempts were generally successful at overcoming the problem. Our three main strategies are described below:

1. Using other loss functions
2. Using a loss function that is a linear combination of other loss functions
3. Using an iterative optimization where each iteration uses a different loss function.

The first method is self-explanatory. Different loss functions will generally have different local minima and landscapes and so other loss functions could yield better performance i.e. more reliably converge to the best known solution. We tried the following loss functions but they did not make much of a difference in our case.

1. Mean-squared error

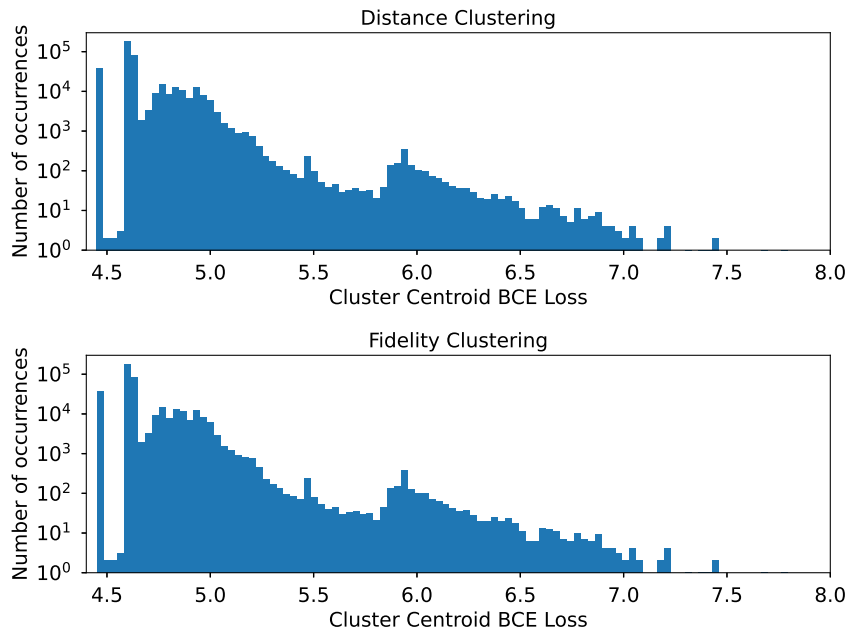


Figure 5. (color online) Normal distribution initialization target. (Top) The distance clustering histogram. (Bottom) The fidelity clustering histogram. Although they look almost identical, there are in fact slight numerical differences.

2. Mean absolute error
3. Huber loss
4. Log-Cosh
5. Fidelity loss i.e. using the state fidelity between the current state and the target state
6. Trace loss i.e. using the trace distance between the current state and the target state

The second method was an attempt to ‘average’ out the loss functions so that the optimizer would be less likely to get stuck in local minima. The challenge here is that loss functions are not easily combined as their absolute values can vary significantly. For example, some are unbounded (e.g. BCE) while others are bounded (e.g. fidelity loss). An attempt to use an equal weight on each loss function (i.e. the arithmetic mean of all of the loss functions) did not help in reliably attaining the best known solution. The weights themselves can probably be machine learned, but this only serves to complicate the problem even further.

Our third method tried to leverage on the intuition that the global minimum should be unique across all loss functions. In this method, the optimizer would start from a random point and would attempt to minimize one loss function. This would converge on (most likely) that loss function’s local minimum. This set of ‘optimized’ parameters would then be the starting point (rather than some random parameters) for the next optimization iteration, utilizing a different loss function. This process is then repeated using different loss functions and the hope is that this helps the optimizer escape local minima. We show the result for a particular attempt using the BCE-trace-fidelity (BTF) loss for 100,000 random points which is representative of other attempts. To clarify the notation, BTF loss means that the BCE loss function was used first, followed by trace loss and then fidelity loss. Note that a circular entanglement strategy was used here as we experienced better results using it for the normal distribution cases (at least for a fewer number of qubits). The solution that was converged upon almost 67% of the time is shown in Fig 6.

This result could mean that such an initialization is not possible with this circuit topology, or that the parameter landscape is simply too complicated and 3 loss functions is insufficient to help the learning algorithm converge on the global minimum. It should also be noted that the runtime for this method would increase linearly with every added loss function as the optimization process is being repeated for every additional loss function.

Another method that was attempted was a small improvement to the previous method of an iterative optimization technique. It also gave us some insight into the ‘agreement’ of the local minima across different loss functions. Rather than using the optimizer sequentially and, in some sense, letting the last loss function in the sequence determine the solution, we could run this iterative optimization scheme until *all* the loss functions agree on the solution. Apart

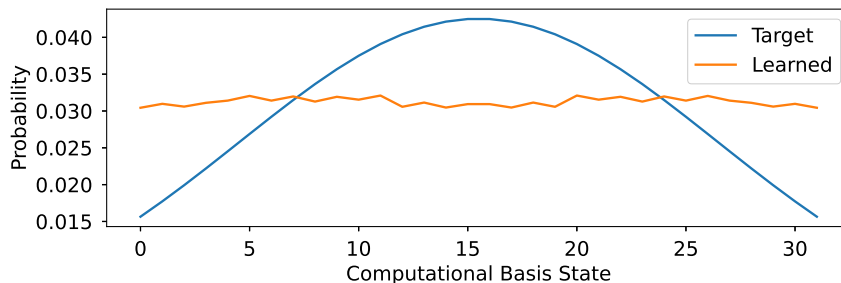


Figure 6. (color online) The most common result achieved (almost 67% of the time) using the BTF loss function sequence. The blue solid line shows the target distribution while the orange line gives the final output of the variational circuit.

from the runtime getting out of hand and genuinely negating any advantage of a quantum algorithm, we also found that we did not always land on the best-known solution even with this method. Although many of the local minima were not shared across loss functions, it seemed that enough of them were common across different loss functions. One could possibly try this method with more and more loss functions to increase the likelihood of convergence to the global minimum, but this was not explored due to the extensive computational requirements.

ACKNOWLEDGMENTS

The Python libraries Dask [1], CuPy [2] and Numba [3], as well as the computing cluster from the A*STAR Computational Resource Center (A*CRC) were used extensively to accelerate and parallelize the ‘exhaustive’ search efforts and clustering of solutions. Qiskit [4] was used for the quantum circuit simulations.

-
- [1] Dask Development Team, *Dask: Library for dynamic task scheduling* (2016).
 - [2] R. Okuta, Y. Unno, D. Nishino, S. Hido, and C. Loomis, Cupy: A numpy-compatible library for nvidia gpu calculations, in *Proceedings of Workshop on Machine Learning Systems (LearningSys) in The Thirty-first Annual Conference on Neural Information Processing Systems* (2017).
 - [3] S. K. Lam, A. Pitrou, and S. Seibert, Numba: A llvm-based python jit compiler, in *Proceedings of the Second Workshop on the LLVM Compiler Infrastructure in HPC*, LLVM ’15 (Association for Computing Machinery, New York, NY, USA, 2015).
 - [4] M. S. Anis *et al.*, *Qiskit: An open-source framework for quantum computing* (2021).